Exponent for the power-law relation between activation energy for dislocation nucleation and applied stress

Anik H. M. Faisal
Department of Mechanical Engineering, Colorado State University, Fort Collins, Colorado 80523, USA

Christopher R. Weinberger
Department of Mechanical Engineering, Colorado State University, Fort Collins, Colorado 80523, USA
and School of Advanced Materials Discovery, Colorado State University, Fort Collins, Colorado 80523, USA

(Received 6 June 2019; published 2 October 2019)

The strength of defect-free crystalline materials is known to be close to the theoretical strength of the material and is typically governed by the nucleation of dislocations. Dislocation nucleation is controlled by the energy barrier associated with the nucleation process, which is a function of both the temperature and stress. Previous work has suggested that the energy barrier decreases with stress towards zero as a power-law relationship and that there may be an exponent with universal value for nucleation. In this paper, we analyze atomistic simulations and continuum models to determine if such a universal exponent exists. Fitting of all available atomistic data to the power-law expression does not yield evidence of a universal power-law behavior. The examination of continuum models, however, provides particular interesting insight. Sufficiently far away from the athermal limit, the energy barrier decays with an effective exponent greater than one such that both the energy barrier and activation volume decrease. However, very close to the athermal limit, the activation volume diverges, due to a divergent activation area of the dislocation loop, resulting in a limiting exponent around 0.5. The divergent activation volume is a result of including the generalized stacking fault energy and allowing the Burgers vector to go to zero during nucleation. These results further provide insight into strategies for empirically modeling the activation energy and activation volume, because they contradict the idea that the activation volume goes to zero, which is currently assumed in most empirical forms of the activation energy.

DOI: 10.1103/PhysRevMaterials.3.103601

I. INTRODUCTION

Dislocations, line defects in crystals, are central to our understanding of plastic deformation and mechanical strength of crystalline materials. While bulk plasticity is well described by continuum plasticity, it is well established that the rules of plasticity change as crystal dimensions are reduced in the microrange and the strength of materials becomes size dependent [1,2]. This idea was examined by the works of Brenner [3,4] on metallic whiskers and has been examined more thoroughly by the microcompression and tension tests on focus ion-beam (FIB) milled micropillars [5–7].

This interest in size affected flow created significant interest in how pristine (defect free) materials would respond to mechanical loading and when a transition between size affected flow and dislocation nucleation would occur [8,9]. This has led to the investigation of the strength of metallic nanowires [10–16], nanoparticles [17–19], and other nanostructured materials [8,20,21]. The strength of many of these materials, especially the nanowires, has been shown to approach the theoretical strength of the materials [16,22,23]. Finally, dislocation nucleation also occurs during nanoindentation and can be attributed, sometimes, to the pop-in events noted in load-displacement curves [24–26].

Molecular dynamics simulations have been instrumental in understanding the mechanisms of dislocation emission and evolution in nanostructures [27,28] which have, in conjunction with the aforementioned experiments, provided significant insight into plastic flow at small scales. However, the difference in strain rates between molecular dynamics and experiments is often many orders of magnitude, which raises a concern as to the exact nature of the predictions of this method. This, in turn, has created interest in exploring dislocation emission as a classical nucleation process. From this viewpoint, dislocation nucleation occurs when there is sufficient energy and time, aided by applied stress, for the dislocation to overcome the free energy barrier preventing its spontaneous nucleation. The nucleation rate, following transition state theory, is

$$\nu = N\nu_0 \exp\left(-\frac{\Delta G^*(\sigma, T)}{k_B T}\right) \tag{1}$$

where N is the number of nucleation sites, ν_0 is a frequency prefactor, ΔG^* is the activation Gibbs free energy, and k_B is Boltzmann's constant [20,29]. The nucleation rate, according to Eq. (1), is strongly dependent on the activation free energy for dislocation nucleation and thus an understanding of dislocation nucleation is tied to the stress and temperature dependence of this activation energy. Zhu *et al.* [30] used the free end nudged-elastic-band method (a chain-of-states method) to examine the internal energy barrier for dislocation nucleation in a copper nanowire as a function of stress. The authors found, as expected, that the activation energy was a

strong function of stress and they fit their atomistic results to an empirical equation:

$$\Delta E^*(\sigma) = E_0\left[1 - \frac{\sigma}{\sigma_0}\right]^{\alpha}, \tag{2}$$

where E_0 and α are fitting parameters, σ is the applied stress, and σ_0 is the athermal strength. This form comes from general empirical models for activation energies used in the literature [31]. However, this expression was only fit to activation internal energies (or enthalpies) at 0 K. To account for finite temperature, Zhu *et al.* used the thermodynamic compensation law (Meyer-Neldel rule) so that the activation free energy can be written as

$$\Delta A^*(\sigma, T) = E_0\left[1 - \frac{\sigma}{\sigma_0}\right]^{\alpha}\left(1 - \frac{T}{T_m}\right), \tag{3}$$

where T_m is a characteristic temperature at which the energy barrier vanishes for all stresses. Zhu *et al.* then extended nucleation equation [Eq. (1)] to predict the most probable nucleation stress as

$$\frac{\Delta G^*(\sigma, T)}{k_B T} = \ln\frac{k_B T N \nu_0}{\mathrm{Y}\dot{\epsilon}\Omega(\sigma, T)}, \tag{4}$$

where Y is the Young's modulus of the material, $\dot{\epsilon}$ is the applied strain rate, and Ω is the activation volume defined as $\Omega = -\frac{d\Delta G^*}{d\sigma}$.

Ryu *et al.* [32] reexamined the same copper nanowire nucleation problem to specifically address the temperature dependence and the thermodynamic compensation law using umbrella sampling to directly calculate the activation free energies. The authors demonstrated that the activation Gibbs free energy and Helmholtz free energy are equal, $\Delta G^* \approx \Delta A^*$ and similarly $\Delta H^* \approx \Delta E^*$. Their work also points out that the thermodynamic compensation law does not always work and that the characteristic temperatures T_m depends on whether the stress or strain is the controlled thermodynamic variable and is not related to the melting temperature (or surface disordering temperature) as is often assumed.

The computation of energy barriers in atomistics, nevertheless, is still a powerful method to gain insight into the nucleation process even if the temperature dependence is still not fully understood. Several investigators have used similar approaches to study dislocation nucleation in gold nanowires [33], from surface steps in fcc metals [34–36], and from pores in aluminum [37]. In addition, these energy barrier calculations have been used in conjunction with continuum models of dislocation nucleation to gain a better understanding of the nucleation phenomenon or to develop better continuum models of dislocation nucleation [38,39].

Despite the interest in calculating energy barriers directly from chain-of-state atomistic calculations or similar methods, these approaches are often expensive and difficult to use. Thus, it is desirable to determine if such information can be obtained from direct atomistic simulations. In an attempt to solve this problem, recently Chachamovitz *et al.* [40] introduced a method to extract the activation free energies from direct molecular dynamics (MD) simulations by examining statistical distribution of nucleation strengths as a function of temperature during constant stress rate simulations. The key point the authors make is that if we assume the nucleation rate follows Eq. (1), then the cumulative distribution function of failure is

$$F(\sigma, T) = 1 - \exp\left[-\frac{N\nu_0}{\dot{\sigma}}\int_0^{\sigma}\exp[-\beta\Delta G^*(\eta)]d\eta\right], \tag{5}$$

where $\dot{\sigma}$ is the applied stress rate and $\beta = \frac{1}{k_B T}$. This theoretical cumulative distribution function can then be fit to cumulative distribution functions determined from direct MD simulations as long as a functional form of ΔG^* is assumed. The authors further argue that the activation volume can be directly related to the standard deviation of the nucleation strengths, which simplifies the parametrization of ΔG^*. For convenience, they assume a functional form of

$$\Delta G^*(\sigma, T) = G_0\left[1 - \frac{\sigma}{\sigma_0}\right]^{\alpha}\left(1 - \frac{T}{T_m}\right) \tag{6}$$

with G_0, α, and T_m (as well as ν_0) determined from numerical fitting of the cumulative distribution functions.

Chachamovitz *et al.* [40] used this method to examine nucleation in their molybdenum nanoparticles and found that the exponent, α, was approximately 1.68. They noted that this exponent was close to the value of 1.5 that has been argued to characterize plastic flow associated with dislocation glide in bulk crystals near the yield point [41–43]. This led to a hypothesis that perhaps an exponent of around 1.5 is a universal exponent for dislocation nucleation near the point of spontaneous nucleation, i.e., the athermal limit. One key point to make by assuming such an exponent is that this implies the activation volume goes to zero in the athermal limit, as would be true for any exponent greater than 1.

The postulate of a universal exponent is intriguing and a worthy point of investigation. It is further worth pointing out that the only other exponent determined was 4.1 by Zhu *et al.* which Chachamovitz *et al.* suggested was a result of the predictions accounting for data too far from the athermal limit. Hence, the objective of this paper is to explore the nature of the activation energy as a function of stress. Notably, we will attempt to determine if the exponent α is indeed universal, i.e., does it have specific value for nucleation, and generally should the activation volume approach zero as the stress approaches the athermal limit. To this end, we analyze atomistic data published in the open literature to determine if there is a universal trend. In addition, we will also investigate the energy barriers as a function of stress using continuum models to understand how dislocation nucleation behaves in the athermal limit of spontaneous nucleation.

II. ANALYSIS OF MD SIMULATION RESULTS AND THE EXPONENT α

The first objective of this study is to determine if atomistic simulations support a universal stress exponent. To this end, we examined existing atomistic simulation data for the activation free energy as a function of stress. We fit the activation free energy data from Zhu *et al.* [8], Aubry *et al.* [38], Jennings *et al.* [39], and Weinberger *et al.* [33] to Eq. (2) in order to extract the exponent. To determine α, we used a nonlinear fitting procedure to minimize the mean-square error between the atomistic energy barrier data and the power-law model. An example of this fit is shown in Fig. 1(a) for a Cu nanowire

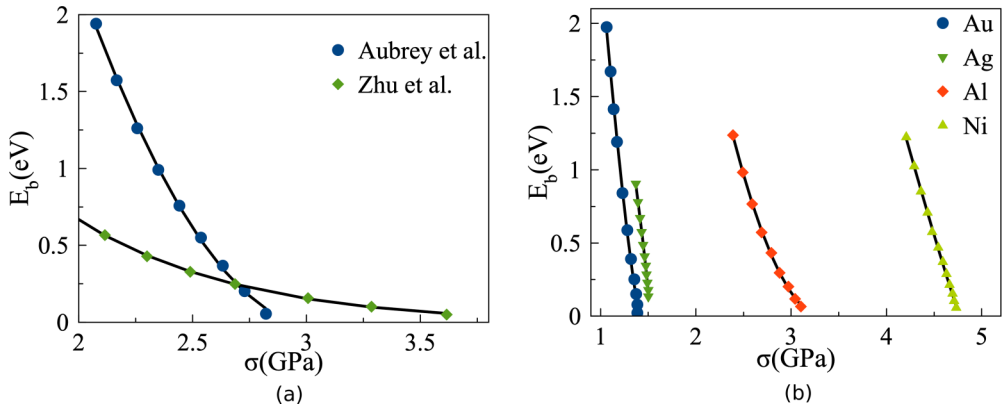

FIG. 1. (a) The energy barrier vs stress for Cu under pure shear (Aubry *et al.*) and compression (Zhu *et al.*) (b) The energy barrier vs stress for Au, Ag, Al, and Ni (Jennings *et al.*).

under pure shear (Aubry *et al.*) and in Fig. 1(b) for a Cu nanowire under uniaxial compression (Zhu *et al.*). For the pure shear data of Jennings *et al.*, σ_0 was included as a free variable in the fitting as no such value was reported by the authors. For the rest of the data, σ_0 was fixed based on previous reported values. In some cases, such as the data of Zhu *et al.*, α is sensitive to the inclusion of σ_0 due to the lack of data near the ideal strength limit. This sensitivity suggests that α may not be an ideal parameter for characterizing the energy barrier beyond an empirical fit.

Table I lists the fitting parameters for the surveyed atomistic data. The exponent α for the nanowires exhibits a wide range of values under uniaxial loading from 1.4 to 5.8 while under pure shear the α values range from 0.8 to 1.9. Clearly, these data do not support a hypothesis that α may have a universal value over the stress range that we have considered. Furthermore, we see that in some cases, especially in pure shear, some of the exponents are close to 1 and in one case, Ag, is less than 1. The case of silver is intriguing because the exponent actually implies a divergent activation volume as the stress approaches the athermal limit, a point that will become important later. The lack of a universal exponent in our data, however, does not completely rule out the hypothesis of Chachamovitz *et al.* as their suggestion should be limited to the athermal limit. However, in many of the atomistic results, it would appear that the activation energies approach the athermal limit with a constant slope, or an exponent of 1, rather than a slope of 0 which is necessary for α to be greater than 1.

III. CONTINUUM MODELS

Since the power-law fitting of the atomistic data does not indicate any universal behavior of the exponent value but is perhaps limited in scope, we proceed to the analysis of continuum models for dislocation nucleation. The continuum models have the advantage of greatly reducing the complexity of the problem to just a few variables, which makes the solutions expedient and potentially quite general. Furthermore, these models will be much easier to examine numerically in the limit as the stress approaches its athermal limit. However, it is important to note that continuum models can also introduce artifacts associated with continuum approximations and this must be kept in mind when analyzing and generalizing the results of such models.

To start, we first examine a continuum model for the nucleation of a circular dislocation under pure shear. While we know that dislocations will not nucleate as a perfect

TABLE I. The best fit parameters for Eq. (2) for the atomistic data surveyed in the literature.

Metal	Reference	Loading condition	σ_0 (GPa)	α
Cu	Zhu *et al.*	compression	5.2	4.1
Cu	Aubry *et al.*	pure shear	3.0	1.8
Au	Jennings *et al.*	pure shear	1.4	1.3
Ag			1.5	0.8
Al			3.3	1.9
Ni			4.8	1.1
Au	Weinberger *et al.*	⟨100⟩ compression rectangular cross section	1.7	2.6
		⟨100⟩ compression circular cross section	1.8	1.4
		⟨100⟩ tension rectangular cross section	4.5	4.8
		⟨100⟩ tension circular cross section	4.6	2.1
		⟨110⟩ compression rectangular cross section	18.4	5.8
		⟨110⟩ compression circular cross section	21.8	4.6
		⟨110⟩ tension circular cross section	3.4	1.5

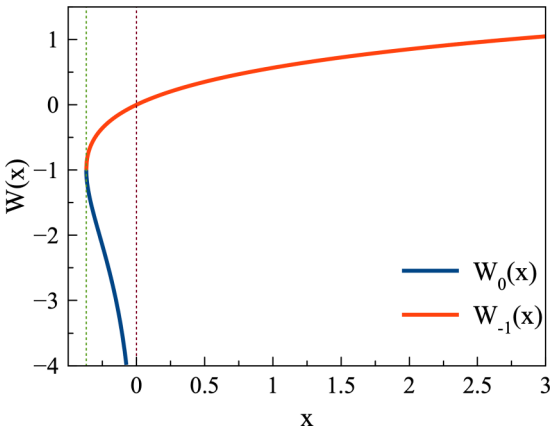

FIG. 2. The real valued Lambert W function with branches $\mathbf{W}_0$ and $\mathbf{W}_{-1}$ [44].

circular loop, this assumption makes the model slightly simpler without compromising too much of the physics. Our approach follows the method of Aubry *et al.* [38], which is an adaptation of the model in Anderson *et al.* [29], which includes the energy of the nucleating dislocation line with a constant Burgers vector. The model we will analyze here only differs from that of Aubry *et al.* in the assumed form of the line energy which is taken from [39]

$$\Delta G(\tau, R) = \frac{\mu b^2}{4}\frac{2-\nu}{1-\nu} R \ln\frac{R}{r_c} - \tau b \pi R^2, \tag{7}$$

where ΔG represents the change in Gibbs free energy due to the formation of the dislocation loop, μ is the shear modulus, ν is the Poisson's ratio, R is the dislocation loop radius, r_c is the dislocation core radius, τ is the applied shear stress, and b is the Burgers vector of the nucleating dislocation. The activation Gibbs free energy, $\Delta G^*(\tau)$, is typically taken as the saddle of the $\Delta G(R, \tau)$ function and can be found by solving R as a function of τ by finding the maximum of ΔG^* with respect to R. This saddle can be found by solving $\frac{\partial \Delta G}{\partial R}(R, \tau) = 0$, which establishes the critical radius R^* for the applied stress τ. Solving for R^* gives an implicit equation:

$$\frac{R^*}{r_c} = A\left[\ln\frac{R^*}{r_c} + 1\right], \tag{8}$$

where $A = \frac{\mu b(2-\nu)}{8\pi r_c \tau(1-\nu)}$. An analytical solution for Eq. (8) is possible in the form of

$$\frac{R^*}{r_c} = -A\mathbf{W}\left(-\frac{1}{Ae}\right), \tag{9}$$

where $\mathbf{W}(x)$ is the Lambert's $\mathbf{W}$ function or the product log function. Lambert's $\mathbf{W}$ function is a complex set of functions with an infinite number of branches with only two of them being real valued. If x is real, then for $\frac{-1}{e} \leqslant x < 0$ there are two possible real values of $\mathbf{W}(x)$, as illustrated in Fig. 2. The branch satisfying $-1 \leqslant \mathbf{W}(x)$ is denoted as $\mathbf{W}_0(x)$ and is referred to as the principal branch while the branch satisfying $\mathbf{W}(x) \leqslant -1$ is denoted as $\mathbf{W}_{-1}(x)$ in the literature [45].

From $\frac{\partial \Delta G}{\partial R}(R, \tau) = 0$, we can define τ^* as

$$\tau^* = \frac{\mu b(2-\nu)}{8\pi R^*(1-\nu)}\left[\ln\frac{R^*}{r_c} + 1\right]; \tag{10}$$

substituting this τ^* into Eq. (7) allows us to express the saddle ΔG^* as a function of R^* as

$$\Delta G^* = \frac{\mu b^2(2-\nu)}{8(1-\nu)} R^*\left[\ln\frac{R^*}{r_c} - 1\right]. \tag{11}$$

When $\Delta G^* = 0$, then we have spontaneous nucleation which corresponds to the ideal strength τ_0. From Eq. (11), this will occur when $[\ln\frac{R^*}{r_c} - 1] = 0$, which results in $R^* = er_c$. Substituting $R^* = er_c$ in Eq. (10), the athermal strength, or ideal strength, τ_0 can be determined as

$$\tau_0 = \frac{\mu b(2-\nu)}{8\pi(1-\nu)}\frac{2}{er_c}. \tag{12}$$

Using Eq. (9) and the definition of τ_0 we can determine the relationship between R^* and τ as

$$R^* = -\frac{er_c}{2}\frac{1}{y}\mathbf{W}\left(\frac{-2y}{e^2}\right), \tag{13}$$

where $y = \frac{\tau}{\tau_0}$. Now, substituting the expression for R^* from Eq. (13) in Eq. (11) we have

$$\Delta G^*(\tau) = \frac{\mu b^2(2-\nu)e}{8(1-\nu)}\left[-\frac{r_c}{2y}\mathbf{W}\left(\frac{-2y}{e^2}\right)\right] \times\left\{\ln\left[-\frac{e}{2y}\mathbf{W}\left(\frac{-2y}{e^2}\right)\right] - 1\right\}. \tag{14}$$

As discussed above and illustrated in Fig. 2, the real valued branches of the Lambert-W function are $\mathbf{W}_0$ and $\mathbf{W}_{-1}$. We consider the $\mathbf{W}_{-1}$ branch as it has been found to be the solution to other dislocation problems [44] and provides positive values of the change in Gibbs free energy here. We note that $\mathbf{W}_{-1}(\frac{-2y}{e^2})$ is infinitely differentiable at $y = 1$ and thus Equation (14) has a power series expansion. This means that α must be a non-negative integer. To determine the value of α as $\tau \to \tau_0$, we expand ΔG^* about $\tau = \tau_0$ as

$$\Delta G^*(\tau) = G_0\left[\left(1-\frac{\tau}{\tau_0}\right) + 2\left(1-\frac{\tau}{\tau_0}\right)^2 + \frac{8}{3}\left(1-\frac{\tau}{\tau_0}\right)^3 + \frac{10}{3}\left(1-\frac{\tau}{\tau_0}\right)^4 + \mathcal{O}\left(1-\frac{\tau}{\tau_0}\right)^5\right], \tag{15}$$

where $G_0 = \frac{\mu b^2(2-\nu)er_c}{8(1-\nu)}$. The power-series expansion clearly demonstrates that $\alpha \to 1$ as $\tau \to \tau_0$. Detailed derivation of this power-series expansion can be found in the Supplemental Material (Sec. I) [46]. For stress values less than τ_0, an empirical fit of $\Delta G = G_0(1-\frac{\tau}{\tau_0})^\alpha$ would give rise to an $\alpha > 0$. The activation volume can be analytically derived, since $b =$ constant, as

$$\Omega = \pi R^2 b = \frac{e^2 r_c^2}{4}\frac{\tau_0^2}{\tau^2}\mathbf{W}_{-1}^2\left(-\frac{2\tau}{e^2\tau_0}\right)\pi b = \frac{1}{4}e^2 r_c^2 \pi b \mathbf{W}_{-1}^2\left(-\frac{2\tau}{e^2\tau_0}\right).$$

In the limit $\tau \to \tau_0$, Ω approaches a constant:

$$\Omega(\tau = \tau_0) = e^2 r_c^2 \pi b. \tag{16}$$

This result contradicts the postulate of an exponent of 1.5, but also assumes that the activation free energy is referenced to a loop of zero radius. This reference is problematic because a

dislocation of zero radius is a local maximum as the energy initially decreases with loop growth and reaches a real local minimum of finite radius before it increases again to the saddle. This is important because the universal exponent of 1.5, a result of catastrophe theory [47], is derived by assuming the saddle collides with a local minimum which is not analyzed in the above derivation.

However, this simple model does predict a local minimum and the system can be analyzed as the saddle (or maximum) approaches this local minimum. The -1 branch of the Lambert function corresponds with the saddle (maximum) and thus the other branch, the 0 branch solution we discarded earlier, corresponds to the minimum. Thus, we can define the actual activation Gibbs free energy barrier as

$$\Delta G^{\dagger} = \Delta G^{*}_{-1} - \Delta G^{*}_{0}, \tag{17}$$

where ΔG^{*}_{-1} and ΔG^{*}_{0} can be found by using the $\mathbf{W}_{-1}$ and $\mathbf{W}_{0}$ branches of the Lambert-$\mathbf{W}$ function in Eq. (9) to solve for R^{*} and substituting R^{*} into Eq. (11). In order for ΔG^{*}_{-1} and ΔG^{*}_{0} to collapse and give rise to $\Delta G^{\dagger} = 0$, Eq. (9) needs to be expanded about $\mathbf{W}(-\frac{1}{e})$, the point where $\mathbf{W}_{-1}$ and $\mathbf{W}_{0}$ converge, as shown in Fig. 2. This requires the term $A = \frac{\mu b(2-\nu)}{8\pi r_c \tau(1-\nu)}$ we defined for Eq. (9) to be unity. Since our objective is to analyze the energy barrier near $\tau \to \tau_0$ we have to redefine $\tau_0 = \frac{\mu b(2-\nu)}{8\pi r_c(1-\nu)}$ such that $A = \frac{\tau_0}{\tau}$. With this definition of τ_0 we can rewrite Eq. (9) as

$$R^{*} = -\frac{r_c}{y}\mathbf{W}\left(-\frac{y}{e}\right),$$

where $y = \frac{\tau}{\tau_0}$. Now ΔG^{*}_{-1} and ΔG^{*}_{0} are

$$\Delta G^{*}_{-1} = K\left(\frac{-1}{y}\right)\mathbf{W_{-1}}\left(\frac{-y}{e}\right) \times \left\{\ln\left[\left(\frac{-1}{y}\right)\mathbf{W_{-1}}\left(\frac{-y}{e}\right)\right] - 1\right\},$$

$$\Delta G^{*}_{0} = K\left(\frac{-1}{y}\right)\mathbf{W_{0}}\left(\frac{-y}{e}\right)\left\{\ln\left[\left(\frac{-1}{y}\right)\mathbf{W_{0}}\left(\frac{-y}{e}\right)\right] - 1\right\},$$

where $K = \frac{\mu b^2 r_c(2-\nu)}{8(1-\nu)}$.

A series expansion of $\mathbf{W}_0$ can be done at the branch point by defining $p = \sqrt{2(1-y)}$ where $y = \frac{\tau}{\tau_0}$ resulting in

$$\mathbf{W_0}(z) = -1 + p - \frac{p^2}{3} + \frac{11p^3}{72} + \cdots.$$

For the $\mathbf{W}_{-1}$ branch, a similar series expansion is defined for $p = -\sqrt{2(1-y)}$ [48]. Substituting the series expansion in the equations for ΔG^{*}_{-1} and ΔG^{*}_{0} and taking their differences in Eq. (17) we obtain for $y \to 1$

$$\Delta G^{\dagger} = K\left[\frac{8\sqrt{2}}{3}(1-y)^{3/2}[1-(1-y)+(1-y)^2-\cdots] + \frac{11\sqrt{2}}{54}(1-y)^{5/2}[1-(1-y)+(1-y)^2-\cdots]\right]. \tag{18}$$

The leading term on the right-hand side of the above equation has an exponent of $\frac{3}{2}$ in accordance with the results from [41–43]. Derivation of this power-series expansion can be found in the Supplemental Material (Sec. II) [46]. This result, even though it auspiciously matches the energy barrier scaling prediction from the catastrophe theory, is fortuitous. This is because the conditions under which the universal exponent was derived are not met in this problem. First, the derivation of the universal exponent of $\frac{3}{2}$ assumes smoothness of the free energy barrier near the collapse. However, in this example the free energy is not smooth; it has a branch point at the athermal limit which negates any universal exponent behavior. Thus, we should not expect agreement of the exponents.

Another reason, which is perhaps more important, is that standard catastrophe theory assumes the driving force is assumed to be linear in the reaction coordinate [47]. However, this is not appropriate for dislocation nucleation. The generalized driving force is the stress τ, which in nucleation scales with the area and thus for a circular loop, R^2.

To extend the ideas developed previously in catastrophe theory specifically to dislocation nucleation we consider a general form for the activation Gibbs free energy for nucleation, ΔG^{*} as

$$\Delta G(\tau, R) = f(R) - \tfrac{1}{2}\tau R^2 \tag{19}$$

with the assumption, for a simple model, that the Burgers vector b is a constant. The function $f(R)$ represents the line energy of the dislocation nucleus which presumably is quadratic in R near $R = 0$ and linear in R for large R. We will further assume that the function $f(R)$ is smooth. We have dropped some of the constants (such as a factor of 2π) for simplicity.

The minimum of the function is assumed to occur at $R = 0$ and the saddle can be found by taking $\frac{\partial \Delta G}{\partial R}(R, \tau) = 0$ which results in

$$\tau = \frac{1}{R^{*}} f'(R^{*})$$

and provides a relationship between the stress and radius at the saddle point. This can be substituted back into the Gibbs free energy equation to obtain

$$\Delta G^{*} = f(R^{*}) - \tfrac{1}{2}R^{*} f'(R^{*}). \tag{20}$$

However, again we need to write this equation in terms of τ and the athermal strength τ_0, notably in terms of $(1 - \frac{\tau}{\tau_0})$.

The athermal strength can be defined as stress at which $R^{*} \to 0$. This can be obtained by examining the functional form of $f(R)$ for small R which, based on our previous assumptions, is

$$f(R^{*}) = a_2 R^{*2} + a_3 R^{*3} + a_4 R^{*4} \ldots. \tag{21}$$

Thus, the athermal strength is

$$\tau_0 = \lim_{R^{*}\to 0} \frac{1}{R^{*}} f'(R^{*}) = 2a_2 = f''(0).$$

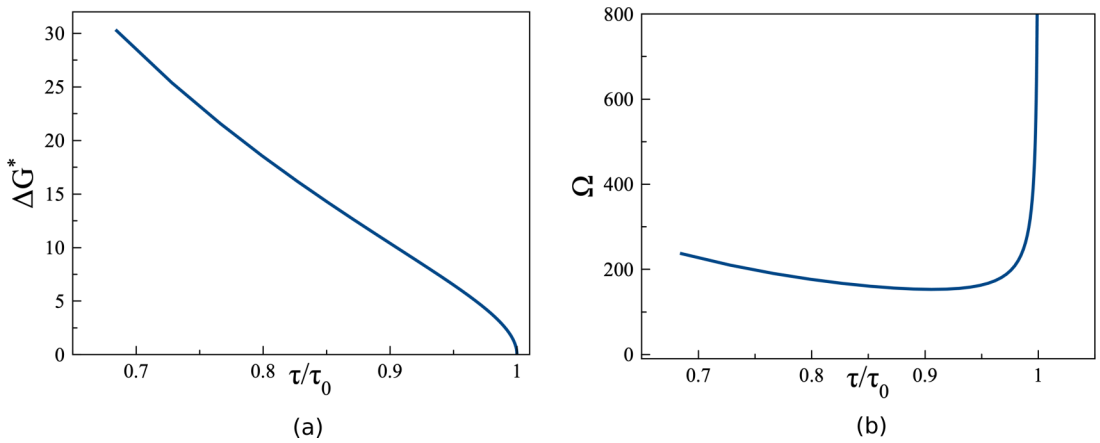

FIG. 3. (a) The activation free energy barrier vs stress behavior for homogeneous dislocation nucleation for the model with variable Burgers vector, i.e., model 2. Activation energies are calculated from Eq. (24). (b) The activation volume vs stress behavior for dislocation nucleation for the augmented model proposed in Eq. (24).

This allows us to write an expression for $(1-\frac{\tau}{\tau_0})$ as

$$1-\frac{\tau}{\tau_0} = 1-\frac{f'(R^*)}{Rf''(R^*)} = -\frac{3}{2}\frac{a_3}{a_2}R^* - 2\frac{a_4}{a_2}R^{*2} - \cdots,$$

which, for sufficiently small R^*, is

$$R^* = -\frac{2}{3}\frac{a_2}{a_3}\left(1-\frac{\tau}{\tau_0}\right). \tag{22}$$

Now, substituting Eq. (22) into Eq. (20) we have

$$\Delta G^*(R^*) = \frac{1}{2}a_3\left[\frac{2}{3}\frac{a_2}{a_3}\left(1-\frac{\tau}{\tau_0}\right)\right]^3 - a_4\left[\frac{2}{3}\frac{a_2}{a_3}\left(1-\frac{\tau}{\tau_0}\right)\right]^4 + \cdots.$$

So, for small R^*

$$\Delta G^* \propto \left(1-\frac{\tau}{\tau_0}\right)^3.$$

If an $f(R)$ is chosen such that $a_3 = 0$, e.g., $f(R)$ is an even function about $R = 0$, then the R^* scales with $(1-\frac{\tau}{\tau_0})^{1/2}$ which results in

$$\Delta G^* \propto \left(1-\frac{\tau}{\tau_0}\right)^2.$$

We verify these two scaling relations, first by choosing an $f(R)$ such that it is consistent with our assumed power-series expansion given in Eq. (21) at $R^* = 0$,

$$f(R) = R\tanh\left(\frac{R}{r_c}\right) + R^2\exp\left(\frac{-R}{r_c}\right) = \left(1+\frac{1}{r_c}\right)R^2 - \frac{R^3}{r_c} + \frac{(3r_c-2)R^4}{6r_c^3} + \cdots.$$

To verify this, the saddle point ($\frac{d\Delta G}{dR} = 0$) is computed relative to the minimum and examined as $\tau \to \tau_0$ which results in a numerical result of

$$\Delta G^* \propto \left(1-\frac{\tau}{\tau_0}\right)^3.$$

The exponential term is included above because it ensures that the equation has a cubic term, resulting in an exponent of 3. If we eliminate this term, $f(R^*) = R^*\tanh(R^*/r_c)$ is

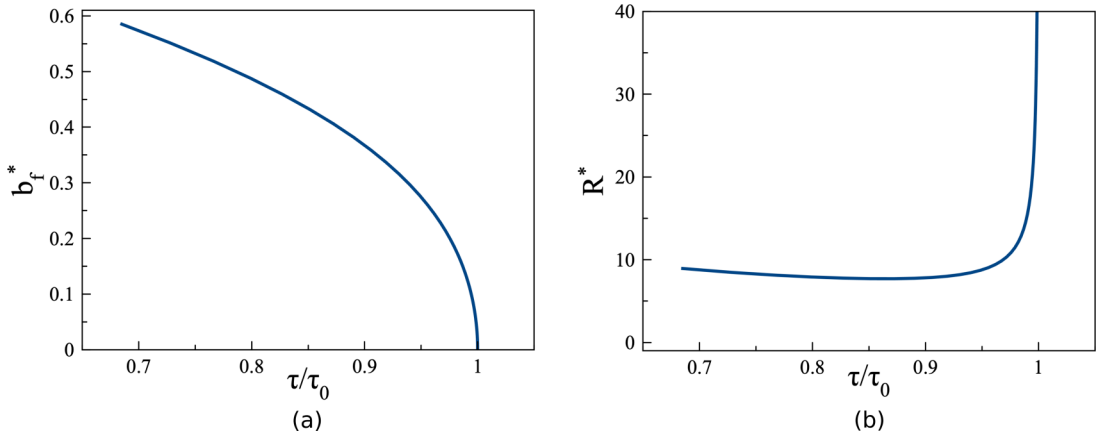

FIG. 4. (a) A plot of Burgers vector corresponding to saddle point b_f^* as a function of $\frac{\tau}{\tau_0}$, asymptotic behavior of the Burgers vector near $\tau \to \tau_0$ can be observed. (b) A plot of critical dislocation loop radius R^* vs $\tau \to \tau_0$. R* diverges as $\tau \to \tau_0$.

even and hence lacks all odd exponents. Numerical analysis demonstrates that the free energy scales as

$$\Delta G^* \propto \left(1 - \frac{\tau}{\tau_0}\right)^2, \tag{23}$$

in agreement with the results of the power-series expansion.

Thus, it is clear that scaling of the activation free energy with the applied stress varies with the choice of line tension term and the continuity of that term at the bifurcation point as we have seen exponents of 2, 3 and, in one special case, 1.5. While this behavior does not contradict the atomistic data presented above (the lack of a universal exponent), this result may still be an artifact of the simple nature of the model. The athermal strength τ_0 is set artificially by a cutoff radius or regularization parameter r_c, instead of the more common notion that $\tau \to \tau_0$ as the Burgers vector, $b \to 0$. This is precluded in the simple model since the Burgers vector is held constant. Thus, our analyzed behavior near $\tau = \tau_0$ may be an artifact of fixing the Burgers vector and an improved model where b is a variable is needed to better understand how ΔG^* should behave near the athermal limit.

To examine the shortcomings of the first continuum model, we also analyze an augmented model where the variable Burgers vector b_f is allowed to vary between 0 and b_0, again following the ideas of Aubry *et al.* but with a line tension term of $R\tanh(R/r_c)$ which is the same $f(R)$ we have used in our generalized simple model that produces $\alpha = 2$. The change in free energy in this model due to the nucleation of a circular dislocation loop is

$$\Delta G(\tau, R, b_f) = \frac{\mu b_f^2}{4}\frac{2-\nu}{1-\nu} R \tanh\frac{R}{r_c} - \tau b_f \pi R^2 + \pi R^2[\gamma(u_0 + b_f) - \gamma(u_0)], \tag{24}$$

where γ is the generalized stacking fault (GSF) energy and the displacement u_0 along the Burgers vector direction can be determined by equating the derivative of the GSF energy and the applied stress: $\frac{d\gamma}{du}|_{u_0} - \tau = 0$ [39]. For the purpose of examining general nucleation, we choose to first analyze the nucleation of a perfect dislocation. In this case, the GSF curve can be readily modeled with a sinusoidal function as $\gamma(u) = \frac{\gamma_0}{2}[1 - \cos(\frac{2\pi u}{b_0})]$. We were unable to find an analytical solution for the activation free energy, so a numerical approach is used. In order to numerically solve for the saddle point ΔG^*, the material constants were nondimensionalized in the above equation [Eq. (24)] as follows: $\mu = 4\pi^2$, $\nu = 0.0$, $b_0 = 1.0$, $r_c = 1.0$, $\gamma_0 = \frac{1}{2\pi}$. τ_0 can be determined by finding the maximum stress the crystal can withstand, defined by the GSF curve, prior to rigid sliding of the crystal. This is the maximum of $\frac{d\gamma}{du}$, which can be solved analytically as $\tau_0 = \pi\frac{\gamma_0}{b_0}$. The value of τ can be related to the GSF curve as noted above, as $\tau = \frac{d\gamma}{du}|_{u_0}$.

Now, to find the activation Gibbs free energy ΔG^* which is the saddle point of $\Delta G(b_f, R, \tau)$ we differentiate Eq. (24) with respect to both R and b_f. Then, we set $\frac{\partial \Delta G}{\partial b_f} = 0$ and $\frac{\partial \Delta G}{\partial R} = 0$. The two equations $\frac{\partial \Delta G}{\partial R} = 0$ and $\frac{\partial \Delta G}{\partial b} = 0$ were numerically solved using the Newton-Raphson method.

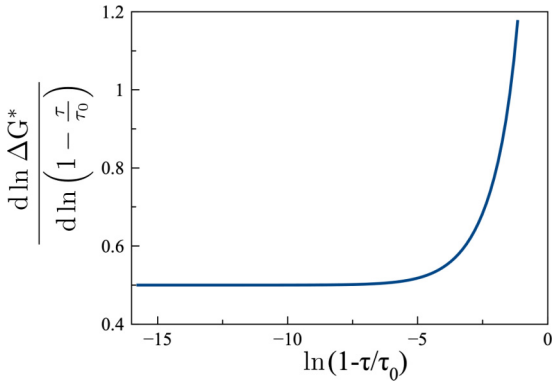

FIG. 5. A log-log plot of $\frac{d\ln\Delta G^*}{d\ln(1-\frac{\tau}{\tau_0})}$ as a function of $(1 - \frac{\tau}{\tau_0})$ for the augmented model of Eq. (24). The exponent α approaches a value of 0.5 as $\tau \to \tau_0$.

Figure 3(a) shows the behavior of the activation free energy as computed by our numerical solution. As $\tau \to \tau_0$ we can see in this augmented model that the activation free energy abruptly drops to zero at τ_0, which in this case is defined as $\frac{d\gamma}{du}|_{\max}$. This behavior implies

$$\lim_{\tau\to\tau_0} \frac{\partial \Delta G^*}{\partial \tau} \to -\infty.$$

To verify this behavior, we note that the activation volume can be directly computed from $\Omega = -\frac{\partial \Delta G^*}{\partial \tau}$, or

$$\Omega = \pi R^2 b_f - \pi R^2\left[\frac{\partial \gamma(u_0 + b_f)}{\partial \tau} - \frac{\partial \gamma(u_0)}{\partial \tau}\right] = \pi R^2 b_f - \pi R^2\left(\left.\frac{d^2\gamma}{du^2}\right|_{u_0}\right)^{-1}\left[\left.\frac{d\gamma}{du}\right|_{u_0+b} - \left.\frac{d\gamma}{du}\right|_{u_0}\right]. \tag{25}$$

It is interesting to note that the activation volume, in this case, is not simply the dislocation loop area times the Burgers vector. It is now altered because of the stress dependent generalized stacking fault energy. This expression also gives us a direct method to compute the activation volume in addition to numerically differentiating the activation free energy.

Figure 3(b) plots the computed activation volume as a function of $\frac{\tau}{\tau_0}$. The activation volume exhibits a shallow decrease as the stress increases in agreement with the shape of the activation free energy up until a critical stress, here about $0.93\tau_0$, at which point it increases and begins to diverge. Note that the activation volume computed from Eq. (25) is indeed the total derivative of the activation energy with respect to stress, which we verified numerically.

If the activation volume does diverge, then the dislocation loop radius at the saddle, R^*, must diverge as well since we expect that b_f^* decreases monotonically. To verify this, Fig. 4 shows the plot of b_f^* and R^* as a function of $\frac{\tau}{\tau_0}$. From this plot we can observe that R^* diverges near $\tau \to \tau_0$ as expected. The rate at which b_f^* approaches zero is faster than the rate R^{*2} diverges which takes ΔG^* to zero since the activation free

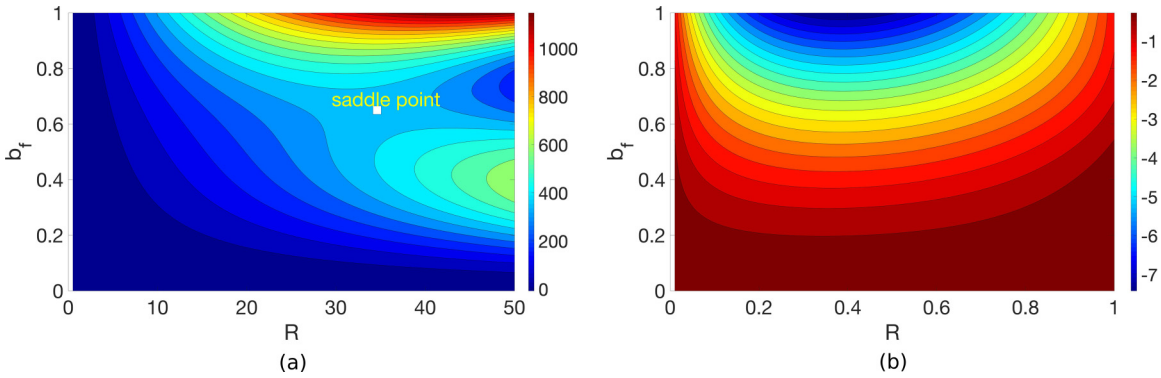

FIG. 6. (a) A contour plot of the free energy surface, $\Delta G(R, b_f)$ modeled as Eq. (26) for $\frac{\tau}{\tau_0} = 0.683$ over the range $R \in [0, 50]$ and $b \in [0, 1]$. (b) Free energy surface over the range $R \in [0, 1]$ and $b \in [0, 1]$.

energy can be written as

$$\Delta G^* = \frac{1}{2}\frac{\mu b_f^{*2}}{4}\frac{2-\nu}{1-\nu}R^*[\tanh(R^*/r_c) + \mathrm{sech}^2(R^*/r_c)]$$

Moreover, as $\tau \to \tau_0$ we expect that $\Omega \to \infty$ as long as

$$b_f - \left(\frac{d^2\gamma}{du^2}\bigg|_{u_0}\right)^{-1}\left[\frac{d\gamma}{du}\bigg|_{u_0+b} - \frac{d\gamma}{du}\bigg|_{u_0}\right] \to 0$$

slower than $R^{*2} \to \infty$, which is evidently true given the results in Fig. 4.

Now that we have ΔG^* as a function of τ numerically, we can compare its behavior to the power-law form. Near the athermal limit, $\tau \to \tau_0$, we can see that $\alpha < 1$ because $\Omega \to \infty$. However, we cannot simply fit the power-law behavior with a single α value. So, to determine the exponent at distinct stress regimes, we examine the behavior of $\frac{d\ln(\Delta G^*)}{d\ln(1-\tau/\tau_0)}$, which is plotted as a function of $\ln(1-\tau/\tau_0)$ in Fig. 5. This plot shows that as $\tau \to \tau_0$, $\frac{d\ln(\Delta G^*)}{d\ln(1-\tau/\tau_0)}$ approaches 0.5, which establishes that ΔG^* is $\propto (1-\frac{\tau}{\tau_0})^{1/2}$, i.e., $\alpha = \frac{1}{2}$. Similar analysis can be carried out on R^* and b_f^*, which gives a result that $b_f \propto (1-\frac{\tau}{\tau_0})^{1/2}$ and $R^* \propto (1-\frac{\tau}{\tau_0})^{-1/2}$.

To explore how the line tension argument affects this new exponent α, we carried out a similar numerical analysis of the augmented model with an alternative line energy term which is the same $f(R)$ we have used in our generalized simple model that produces $\alpha = 3$ as

$$\Delta G(\tau, R, b_f) = \frac{\mu b_f^2}{4}\frac{2-\nu}{1-\nu}[R\tanh(R/r_c) + R^2\exp(-R/r_c)] - \tau b_f \pi R^2 + \pi R^2[\gamma(u_0+b_f) - \gamma(u_0)].$$

A similar analysis of this model also gives rise to $\alpha = 0.5$ for this version of the augmented model. Finally, we have also analyzed the case in which the dislocation energy term is linear in R, i.e., $\frac{\mu b_f^2}{4}\frac{2-\nu}{1-\nu}R$, which also results in $\alpha = 0.5$. Thus we infer that $\alpha = \frac{1}{2}$ is relatively invariant to the choice of the line tension term as long as ΔG is continuous when the saddle meets the minimum. We further point out that the results are not dependent on the choices of r_c or γ_0 in this model; the exponents remain the same.

At this point, we return to the augmented model proposed by Jennings *et al.* in [39]:

$$\Delta G(\tau, R, b_f) = \frac{\mu b_f^2}{4}\frac{2-\nu}{1-\nu}R\ln\frac{R}{r_c} - \tau b_f \pi R^2 + \pi R^2[\gamma(u_0+b_f) - \gamma(u_0)]. \quad (26)$$

The simple version of this model, which does not include the generalized stacking fault energy penalty term, introduces an artificial minimum. This required the introduction of $\Delta G^\dagger$, which was the difference between the saddle (maximum) and the artificial minimum, which was discontinuous at the

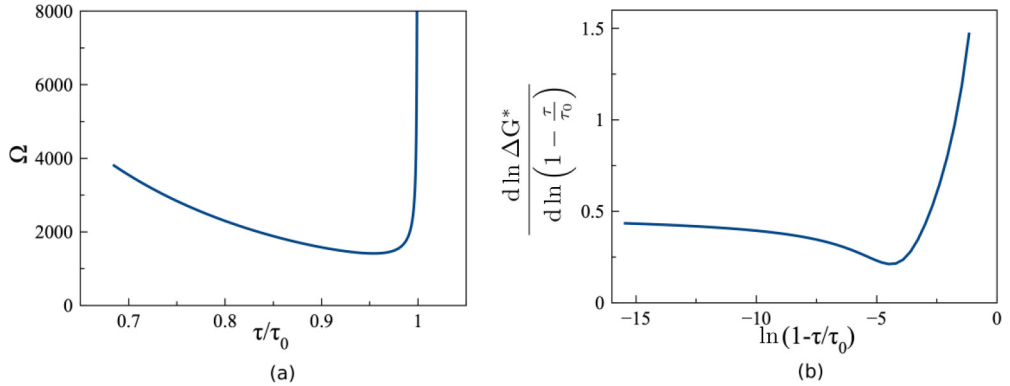

FIG. 7. (a) The activation volume vs stress behavior for dislocation nucleation modeled by Eq. (26). (b) A log-log plot of $\frac{d\ln\Delta G^*}{d\ln(1-\frac{\tau}{\tau_0})}$ as a function of $(1-\frac{\tau}{\tau_0})$ for the augmented model of Eq. (26). The exponent α approaches a value of 0.4 as $\tau \to \tau_0$.

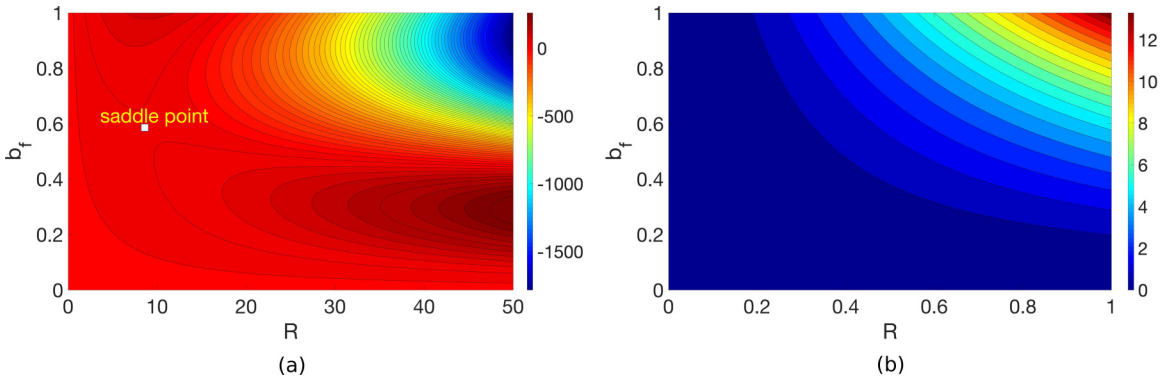

FIG. 8. (a) A contour plot of the free-energy surface $\Delta G(R, b_f)$ modeled as Eq. (24) for $\frac{\tau}{\tau_0} = 0.683$ over the range $R \in [0, 50]$ and $b \in [0, 1]$. (b) Free-energy surface over the range $R \in [0, 1]$ and $b \in [0, 1]$.

athermal limit and resulted in an exponent of 1.5. As we will demonstrate later, the function ΔG as represented by Eq. (26) does not have a local minimum. Instead there is only a saddle point and a local maximum at $(R, b_f) = (0, 0)$ for all $\tau \leqslant \tau_0$. The local minimum artificially introduced by the logarithm term is no longer a minimum but creates a path in which there is no free energy barrier for dislocation nucleation as the Burgers vector can grow unbounded.

To illustrate this behavior, consider a numerical implementation of Eq. (26). For this example, we consider the numerical case where $\tau = 0.684\tau_0$, $\mu = 4\pi^2$, $\nu = 0.0$, $b_0 = 1.0$, $r_c = 1.0$. The GSF term is described by $\gamma(\mathrm{u}) = \frac{\gamma_0}{2}[1 - \cos(\frac{2\pi \mathrm{u}}{\mathrm{b_0}})]$ as before with $\gamma_0 = \frac{1}{2\pi}$. A contour plot of ΔG as a function of R and b is shown Fig. 6 which shows that for small R, as the Burgers vector is increased ΔG continuously decreases [Fig. 6(b)]. While this is certainly mathematically possible, it is often ignored as an artifact in the dislocation model. Nevertheless, it makes the $(R, b_f) = (0, 0)$ a maximum and not a minimum due to the ability to decrease the free energy by increasing R.

Despite the obvious mathematical issues with this model, it is still insightful to examine how the saddle approaches the $(R, b_f) = (0, 0)$ maximum as this has been regularly used in modeling dislocation nucleation. The solution strategy is exactly the same as that used for the other models with varying Burgers vectors. The two key pieces of information obtained from the analysis are shown in Fig. 7, the behavior of the activation volume and a plot of the effective exponent. Just as occurred in the other cases, the activation volume diverges when the stress reaches the athermal limit. Figure 7(b) shows that as the stress reaches the athermal limit, the exponent approaches a value of approximately 0.4, distinctly different from that of the other models with variable Burgers vectors in which the exponent was 0.5. The difference in exponents between the models appears to be a result of the $(R, b_f) = (0, 0)$ point being a maximum in this case, as opposed to a minimum in the case of the other models. To illustrate more clearly the differences in the free-energy models, consider a contour plot of the free energy using the model of Eq. (24) as shown in Fig. 8. This figure shows in this case there is a clear saddle and that the point $(R, b_f) = (0, 0)$ is indeed the local minimum. A zoomed in region near the origin, Fig. 8(b), confirms that the function is a minimum at the origin.

To ensure the generality of our results, we have also computed the exponents for different GSF terms. For example, models of the dislocation nucleation process originally used a GSF term of the form $\gamma(u) = \frac{\gamma_0}{2}[1 - \cos(\frac{2\pi u}{b_0})]$ where b_f represents the Burgers vector of a perfect dislocation. Alternatively, we can also analyze the model with a GSF term that represents the nucleation of a partial dislocation, as Aubry *et al.* did [38]. To achieve this in our numerical implementation in which a continuous GSF is needed, we fit the GSF curve for copper given in [38] using a fifth-order polynomial with the first two coefficients set to zero. This GSF model was implemented into our free-energy calculations and while the numerical values of the free energies changed, the extracted exponents did not.

IV. SUMMARY AND DISCUSSION

For bulk plastic deformation [41,42], dislocation nucleation [40], and transitions from elastic to inelastic deformation [43,47,49–51], it has been proposed that $\Delta G \propto (1 - \tau/\tau_0)^\alpha$ with a universal $\alpha = \frac{3}{2}$. In this work, we examined all previous atomistic data in which the energy barriers were explicitly computed from atomistic chain-of-states methods, and found the exponents varied between 0.8 and 5.8, indicating that there is little support for a universal exponent from such atomistic simulations. However, the analysis was performed on all available data and not necessarily just limited to the athermal limit and as such, we cannot refute a universal exponent for dislocation nucleation from available atomistic data.

To provide additional insight into the behavior of the activation free energy as a function of stress, we analyzed several continuum models of dislocation nucleation. For stress sufficiently far from the athermal limit, it is clear that an empirical model of the form $\Delta G = G_0(1 - \tau/\tau_0)^\alpha$ can be used and will predict a value of $\alpha > 1$, but this value is not a constant and will depend on the range of stresses used in the empirical fit. As for applied stress $\tau \to \tau_0$ the numerical value of the exponent will depend on the assumed form of the line energy as well as how the driving force scales with dislocation loop radius. For a defect-free crystal, where a dislocation has to be nucleated first to induce failure, the applied stress scales with R^{*2} since the stress is applied over the dislocation loop being nucleated. These considerations suggest that the

equation [Eq. (2)] introduced by Zhu *et al.* [8] is best described as an empirical relationship.

In the first class of continuum models we analyzed, the Burgers vector was held constant which allowed us to derive an analytic expressions for the activation free energy and activation volume as a function of stress by setting an artificial athermal strength. In all of the cases analyzed, the exponent was greater than 1 and the activation free energy and activation volume decreased to 0 at the athermal limit. The value of the exponent depended on the form of the line energy. For the line energy that scaled as $R\ln(R/r_c)$, the exponent was $\frac{3}{2}$, a result of the lack of continuity when the saddle collides with the minimum. When the line energy is continuous, the exponent was found to be 3 if the line energy term has third-order power in its expansion and a value of 2 if the first term in the expansion is fourth order. Presumably, other exponents would be found if the expansion of the free energy was missing the fourth-order term in the expansion of the free energy.

In the second class of models, we allow the Burgers vector to change and include an energy penalty associated with the generalized stacking fault energy as a function of the Burgers vector. In this case, if the line energy creates a minimum at $R = 0$ and the function is smooth, the activation volume is found to diverge. The divergence of the activation volume is a result of the critical radius diverging while the Burgers vector goes to zero. The extracted activation energy exponent α is $\frac{1}{2}$. However, if the line energy includes the standard logarithm term, we find that the behavior is similar but that the exponent becomes roughly 0.4.

These exponents appear to violate catastrophe theory as well as our previous results regarding the general nature of exponents in dislocation nucleation. However, we should also note that the exponents derived in this way assume, as noted before, that the free energy is smooth when the saddle approaches the minimum. In the cases when the exponent is less than 1, the radius diverges invalidating the assumptions made regarding smoothness. It is further clear that it is the introduction of the GSF term that causes the radius to diverge while allowing the Burgers vector to go to 0. The GSF term acts to cause the activation free energy to rapidly decrease to 0, which in turn causes the activation volume to diverge.

This raises a question regarding the divergence of the activation volume; can this be physical or is it a numerical artifact? We know that exponents that are larger than 1 as derived in our first class of models in which the Burgers vector is held constant are indeed artifacts of the model. This is because the athermal strength in each case is directly related to r_c, a regularization constant used to create a smooth quadratic local minimum. However, in the cases where the Burgers vector was allowed to change and $R \to \infty$, the result appears to be a physically meaningful result. As τ approaches the ideal strength, $b_f \to 0$ and thus the crystal is able to rigidly shear, which can readily occur over the whole crystal at once and thus physically represents $R \to \infty$. Thus, it is possible to accept the results obtained here on physical grounds, not just mathematical ones.

This then raises the question of what is the correct exponent in the athermal limit, the value of $\frac{1}{2}$ or the value of roughly 0.4. While we cannot say for sure, we can speculate that the value of $\frac{1}{2}$ appears more appropriate. As noted previously, all the models that have a minimum at $(R = 0, b_f = 0)$ also have an exponent of $\frac{1}{2}$. The only exception is the model with the $R\ln(R/r_c)$ line energy term which, as stated before, has some numerical artifacts as a result of the logarithm term. Given that the logarithm may not be representative of the energy for R values less than r_c physically, the free energy near the athermal limit may not be particularly accurate for dislocation nucleation. Thus, we speculate that the exponent of $\frac{1}{2}$ is the most likely correct exponent for dislocation nucleation.

While the detailed continuum models provide some insight into how the activation energy and activation volume behave very close to the athermal limit, these results may not, at first, appear particularly relevant to actually modeling dislocation nucleation. However, these results, in conjunction with the atomistic modeling results, do offer some important insights into empirical modeling of the activation energy equations. To better understand this, consider the empirical activation energy equation proposed by Zhu *et al.* [30]. The assumed form of the activation energy predicts an activation volume of: $\Omega = \frac{E_0\alpha}{\tau_0}(1 - \tau/\tau_0)^{\alpha-1}(1 - T/T_m)$. This particular form almost entirely precludes the possibility of having a constant activation volume at $\tau \to \tau_0$. If we examine the results of our continuum model the activation volume goes to a constant before sharply diverging. Similar conclusions can be drawn by visual examination of the activation energy plots from direct atomistics, as shown earlier: the activation volume appears to approach a constant. This suggest that empirically fitting the activation volume to an equation that enforces the activation volume to go to zero in the athermal limit can cause numerical issues in the modeling dislocation nucleation, especially when the activation volume is determined and integrated to the activation energy. If this is the case, it would appear choosing an empirical form for the activation energy that can accommodate a nonzero activation volume at the athermal limit is beneficial. Such a form has been proposed by Weinberger *et al.* [33], although this is not the only form that one could suggest.

ACKNOWLEDGMENT

C.R.W. and A.H.M.F. gratefully acknowledge support from the Office of Naval Research under Grant No. N00014-17-1-2810.

[1] J. R. Greer and J. T. M. De Hosson, Plasticity in small-sized metallic systems: Intrinsic versus extrinsic size effect, Prog. Mater. Sci. **56**, 654 (2011).

[2] J. A. El-Awady, Unravelling the physics of size-dependent dislocation-mediated plasticity, Nat. Commun. **6**, 5926 (2015).

[3] S. S. Brenner, Tensile strength of whiskers, J. Appl. Phys. **27**, 1484 (1956).

[4] S. Brenner, Plastic deformation of copper and silver whiskers, J. Appl. Phys. **28**, 1023 (1957).

[5] C. Chisholm, H. Bei, M. Lowry, J. Oh, S. S. Asif, O. Warren, Z. Shan, E. P. George, and A. M. Minor, Dislocation starvation

and exhaustion hardening in mo alloy nanofibers, Acta Mater. **60**, 2258 (2012).

[6] M. D. Uchic, D. M. Dimiduk, J. N. Florando, and W. D. Nix, Sample dimensions influence strength and crystal plasticity, Science **305**, 986 (2004).

[7] M. D. Uchic, P. A. Shade, and D. M. Dimiduk, Plasticity of micrometer-scale single crystals in compression, Annu. Rev. Mater. Res. **39**, 361 (2009).

[8] T. Zhu, J. Li, S. Ogata, and S. Yip, Mechanics of ultra-strength materials, MRS Bull. **34**, 167 (2009).

[9] A. T. Jennings, J. Li, and J. R. Greer, Emergence of strain-rate sensitivity in cu nanopillars: Transition from dislocation multiplication to dislocation nucleation, Acta Mater. **59**, 5627 (2011).

[10] J. Wang, Z. Zeng, C. R. Weinberger, Z. Zhang, T. Zhu, and S. X. Mao, *In situ* atomic-scale observation of twinning-dominated deformation in nanoscale body-centred cubic tungsten, Nat. Mater. **14**, 594 (2015).

[11] L. Y. Chen, M.-r. He, J. Shin, G. Richter, and D. S. Gianola, Measuring surface dislocation nucleation in defect-scarce nanostructures, Nat. Mater. **14**, 707 (2015).

[12] Y. Zhu, Q. Qin, F. Xu, F. Fan, Y. Ding, T. Zhang, B. J. Wiley, and Z. L. Wang, Size effects on elasticity, yielding, and fracture of silver nanowires: *In situ* experiments, Phys. Rev. B **85**, 045443 (2012).

[13] H. Zheng, A. Cao, C. R. Weinberger, J. Y. Huang, K. Du, J. Wang, Y. Ma, Y. Xia, and S. X. Mao, Discrete plasticity in sub-10-nm-sized gold crystals, Nat. Commun. **1**, 144 (2010).

[14] B. Wu, A. Heidelberg, and J. J. Boland, Mechanical properties of ultrahigh-strength gold nanowires, Nat. Mater. **4**, 525 (2005).

[15] J.-H. Seo, Y. Yoo, N.-Y. Park, S.-W. Yoon, H. Lee, S. Han, S.-W. Lee, T.-Y. Seong, S.-C. Lee, K.-B. Lee *et al.*, Superplastic deformation of defect-free au nanowires via coherent twin propagation, Nano Lett. **11**, 3499 (2011).

[16] A. Sedlmayr, E. Bitzek, D. S. Gianola, G. Richter, R. Mönig, and O. Kraft, Existence of two twinning-mediated plastic deformation modes in au nanowhiskers, Acta Mater. **60**, 3985 (2012).

[17] D. Mordehai, S.-W. Lee, B. Backes, D. J. Srolovitz, W. D. Nix, and E. Rabkin, Size effect in compression of single-crystal gold microparticles, Acta Mater. **59**, 5202 (2011).

[18] W.-Z. Han, L. Huang, S. Ogata, H. Kimizuka, Z.-C. Yang, C. Weinberger, Q.-J. Li, B.-Y. Liu, X.-X. Zhang, J. Li *et al.*, From "smaller is stronger" to "size-independent strength plateau": Towards measuring the ideal strength of iron, Adv. Mater. **27**, 3385 (2015).

[19] D. Chrobak, N. Tymiak, A. Beaber, O. Ugurlu, W. W. Gerberich, and R. Nowak, Deconfinement leads to changes in the nanoscale plasticity of silicon, Nat. Nanotechnol. **6**, 480 (2011).

[20] J. Li, The mechanics and physics of defect nucleation, MRS Bull. **32**, 151 (2007).

[21] X. Li, Y. Wei, L. Lu, K. Lu, and H. Gao, Dislocation nucleation governed softening and maximum strength in nano-twinned metals, Nature (London) **464**, 877 (2010).

[22] G. Richter, K. Hillerich, D. S. Gianola, R. Monig, O. Kraft, and C. A. Volkert, Ultrahigh strength single crystalline nanowhiskers grown by physical vapor deposition, Nano Lett. **9**, 3048 (2009).

[23] H. Bei, S. Shim, E. P. George, M. K. Miller, E. Herbert, and G. M. Pharr, Compressive strengths of molybdenum alloy micro-pillars prepared using a new technique, Scr. Mater. **57**, 397 (2007).

[24] J. Li, K. J. Van Vliet, T. Zhu, S. Yip, and S. Suresh, Atomistic mechanisms governing elastic limit and incipient plasticity in crystals, Nature (London) **418**, 307 (2002).

[25] C. Schuh, J. Mason, and A. Lund, Quantitative insight into dislocation nucleation from high-temperature nanoindentation experiments, Nat. Mater. **4**, 617 (2005).

[26] P. Schall, I. Cohen, D. A. Weitz, and F. Spaepen, Visualizing dislocation nucleation by indenting colloidal crystals, Nature (London) **440**, 319 (2006).

[27] C. R. Weinberger and W. Cai, Plasticity of metal nanowires, J. Mater. Chem. **22**, 3277 (2012).

[28] H. S. Park and J. A. Zimmerman, Modeling inelasticity and failure in gold nanowires, Phys. Rev. B **72**, 054106 (2005).

[29] P. M. Anderson, J. P. Hirth, and J. Lothe, *Theory of Dislocations* (Cambridge University Press, New York, 2017).

[30] T. Zhu, J. Li, A. Samanta, A. Leach, and K. Gall, Temperature and Strain-Rate Dependence of Surface Dislocation Nucleation, Phys. Rev. Lett. **100**, 025502 (2008).

[31] U. Kocks, A. Argon, and M. Ashby, *Thermodynamics and Kinetics of Slip*, Progress in Materials Science Vol. 19, edited by B. Chalmers, J. W. Christian, and T. B. Massalsk (Oxford University Press, Oxford, UK, 1975).

[32] S. Ryu, K. Kang, and W. Cai, Predicting the dislocation nucleation rate as a function of temperature and stress, J. Mater. Res. **26**, 2335 (2011).

[33] C. R. Weinberger, A. T. Jennings, K. Kang, and J. R. Greer, Atomistic simulations and continuum modeling of dislocation nucleation and strength in gold nanowires, J. Mech. Phys. Solids **60**, 84 (2012).

[34] S. Hara, S. Izumi, and S. Sakai, Reaction pathway analysis for dislocation nucleation from a ni surface step, J. Appl. Phys. **106**, 093507 (2009).

[35] S. Brochard, P. Hirel, L. Pizzagalli, and J. Godet, Elastic limit for surface step dislocation nucleation in face-centered cubic metals: Temperature and step height dependence, Acta Mater. **58**, 4182 (2010).

[36] P. Hirel, J. Godet, S. Brochard, L. Pizzagalli, and P. Beauchamp, Determination of activation parameters for dislocation formation from a surface in fcc metals by atomistic simulations, Phys. Rev. B **78**, 064109 (2008).

[37] L. Nguyen and D. Warner, Improbability of Void Growth in Aluminum Via Dislocation Nucleation Under Typical Laboratory Conditions, Phys. Rev. Lett. **108**, 035501 (2012).

[38] S. Aubry, K. Kang, S. Ryu, and W. Cai, Energy barrier for homogeneous dislocation nucleation: Comparing atomistic and continuum models, Scr. Mater. **64**, 1043 (2011).

[39] A. T. Jennings, C. R. Weinberger, S.-W. Lee, Z. H. Aitken, L. Meza, and J. R. Greer, Modeling dislocation nucleation strengths in pristine metallic nanowires under experimental conditions, Acta Mater. **61**, 2244 (2013).

[40] D. Chachamovitz and D. Mordehai, The stress-dependent activation parameters for dislocation nucleation in molybdenum nanoparticles, Sci. Rep. **8**, 3915 (2018).

[41] R. Becker, Uber die plastizität amorpher und kristalliner fester körper, Phys. Z. **26**, 919 (1925).

[42] J. W. Cahn and F. Nabarro, Thermal activation under shear, Philos. Mag. A **81**, 1409 (2001).

[43] A. Cottrell, Thermally activated plastic glide, Philos. Mag. Lett. **82**, 65 (2002).

[44] A. Braun, K. Briggs, and P. Böni, Analytical solution to matthews' and blakeslee's critical dislocation formation thickness of epitaxially grown thin films, J. Cryst. Growth **241**, 231 (2002).

[45] S. R. Valluri, D. J. Jeffrey, and R. M. Corless, Some applications of the lambert *W* function to physics, Can. J. Phys. **78**, 823 (2000).

[46] See Supplemental Material at http://link.aps.org/supplemental/10.1103/PhysRevMaterials.3.103601 for detailed derivation of Eqs. (15) and (18).

[47] C. E. Maloney and D. J. Lacks, Energy barrier scalings in driven systems, Phys. Rev. E **73**, 061106 (2006).

[48] R. M. Corless, G. H. Gonnet, D. E. Hare, D. J. Jeffrey, and D. E. Knuth, On the lambertw function, Adv. Comput. Math. **5**, 329 (1996).

[49] S. Karmakar, E. Lerner, and I. Procaccia, Statistical physics of the yielding transition in amorphous solids, Phys. Rev. E **82**, 055103(R) (2010).

[50] C. Maloney and A. Lemaitre, Universal Breakdown of Elasticity at the Onset of Material Failure, Phys. Rev. Lett. **93**, 195501 (2004).

[51] D. Rodney, A. Tanguy, and D. Vandembroucq, Modeling the mechanics of amorphous solids at different length scale and time scale, Modell. Simul. Mater. Sci. Eng. **19**, 083001 (2011).